Journal of Alloys and Compounds 507 (2010) 557–562

Contents lists available at ScienceDirect

Journal of Alloys and Compounds

journal homepage: www.elsevier.com/locate/jallcom

# Optical spectroscopy, optical conductivity, dielectric properties and new methods for determining the gap states of CuSe thin films

G.B. Sakr [a], I.S. Yahia [a,*], M. Fadel [a], S.S. Fouad [a], N. Romčević [b]

[a] Physics Department, Faculty of Education, Ain Shams University, Roxy, Cairo, Egypt
[b] Institute of Physics, Pregrevica 118, 11080 Belgrade, Serbia

ARTICLE INFO

*Article history:*
Received 9 March 2010
Received in revised form 4 August 2010
Accepted 5 August 2010
Available online 13 August 2010

*Keywords:*
CuSe
Thin film
Optical dispersion parameters
Dielectric properties
Relaxation time
Optical conductivity
Determination of the gap states

ABSTRACT

The paper describes the structural and optical properties of CuSe thin films. X-ray diffraction pattern indicates that CuSe thin film has an amorphous structure. Transmittance $T(\lambda)$ and reflectance $R(\lambda)$ measurements in the wavelength range (300–1700 nm) were used to calculate the refractive index $n(\lambda)$, the absorption index and the optical dispersion parameters according to Wemple and Didomenico WDD model. The dispersion curve of the refractive index shows an anomalous dispersion in the absorption region and a normal dispersion in the transparent region. The optical bandgap has been estimated and confirmed by four different methods. The value for the direct bandgap for the as-deposited CuSe thin film approximately equals 2.7 eV. The Raman spectroscopy was used to identify and quantify the individual phases presented in the CuSe films.

© 2010 Elsevier B.V. All rights reserved.

## 1. Introduction

The considerable interest of research workers in chalcogenide semiconductors is due to the possibility of their various applications in different fields of electronic devices based on the fact that they combine the characteristic features of the disordered systems and some properties of the crystalline semiconducting materials. They are attracting an extensive attention due to their practical and potential uses in the civil, medical and military areas, especially in the fields of infrared optics, opto-electronics, photonics, fiber optics and novel memory devices. They also show a continuous change in the physical properties with change of chemical composition [1,2].

Chalcogenide materials are of considerable interest as the promising semiconductor for electro-optic devices, thermoelectric devices and optical recording media. Being the promising materials with potential applications, they can be prepared in a variety of ways [3]. Recently chalcogenide glasses have been investigated as infrared transmitting materials to replace single-crystalline germanium for fabricating infrared optical lenses used in the thermal imaging system due to their advantages over crystals of much lower cost, easier fabrication of complex aspheric IR optical lenses and higher chemical stability [4–7]. The use of thin films of chalcogenide glasses has attracted much interest in an expanding variety of applications in various electronic and optoelectronic devices [8]. They exhibit several particular phenomena useful for devices such as electrical switches, memories, image storage, and photo resistors [9].

Metal chalcogenide compounds, having a semiconductor nature, are of considerable technical interest in the field of electronics and electro-optical devices. Intensive research has been performed in the past to study the fabrication and characterization of these compounds in the form of thin films. Thin chalcogenide films are of particular interest for the fabrication of large area photodiode arrays, solar selective coating, solar cells, photoconductors, sensors, etc [10].

Among these chalcogenide materials, copper selenide has been extensively studied with great interest during the past decades. It has a lot of potential application in the fabrication of photovoltaic devices such as window material, super-ionic conductor, electro-optical devices, optical filter, solar cell, lithium ion cells, thermoelectric converter, photo-thermal conversion, electroconductive electrodes, and microwave shielding coating [11,12]. Copper selenide is a metal chalcogenide semiconductor with a wide range of stoichiometric compositions and also with various crystallographic forms for each of these compositions. The synthesis of this material in thin film form has been described by using different deposition method such as chemical bath deposition (CBD) selenisation, flash evaporation, vacuum evaporation and spray method, etc. [10]. Copper (I) selenide exists in widely different crystallographic modifications even at room temperature such

* Corresponding author. Tel.: +20 182848753; fax: +20 22581243.
*E-mail addresses:* dr_isyahia@yahoo.com, isyahia@gmail.com (I.S. Yahia).

0925-8388/$ – see front matter © 2010 Elsevier B.V. All rights reserved.
doi:10.1016/j.jallcom.2010.08.022

as (orthorhombic, monoclinic and cubic) forms, depending on the method of preparation.

In the present study, we attempt to produce a high quality amorphous CuSe thin film. The structure of the obtained film is discussed on the basis of X-ray diffraction data. Some optical characteristics are also reported. The above properties have been reviewed with respect to the results of the Raman spectroscopy. Also, new methods for the determining the bandgap of CuSe thin films were applied.

## 2. Experimental

Copper selenide was supplied from Aldrich Company of purity 99.99%. The alloy was deposited by using Mo boat onto a pre-cleaned glass substrates kept at room temperature (303 K) and a vacuum better than $2 \times 10^{-5}$ Torr using a conventional coating unit (Edwards, E-306 A). The rate of deposition was constant through the evaporation of CuSe thin films and equals 10 nm/s. The film thickness was controlled by using a quartz crystal thickness monitor (FTM4, Edwards). Three different thicknesses (56.75, 79.74 and 172.7 nm) with the same evaporation rate were deposited onto glass substrates.

The structural characterization of CuSe thin film was investigated by using X-ray diffraction pattern. Philips X-ray diffractometer (model X'-Pert) was used for the measurement of utilized monochromatic CuK$\alpha$ radiation operated at 40 kV and 25 mA. The diffraction patterns were recorded automatically with a scanning speed of 2°/min. The chemical composition of the obtained films is checked by the energy dispersive X-ray analysis (EDX) using scanning electronic microscope (Joel 5400). Fully quantitative analysis results were obtained from the spectra by processing the data through ZAF correction program.

Transmittance $T(\lambda)$ and reflectance $R(\lambda)$ were measured simultaneously using F10-VC-EXR (Filmetrics, Inc., San Diego, CA, USA) in the wavelength range 380–1700 nm. Values of thicknesses of the investigated samples were calculated ex situ using the F10-VC-EXR software.

The micro-Raman spectra were taken in the backscattering configuration and analyzed using Jobin Yvon T64000 spectrometer, equipped with nitrogen cooled charge-coupled-device detector. As the excitation source, we used the 514.5 nm line of Ar–iron laser. The spectra were recorded automatically in the wavenumber range 100–800 cm$^{-1}$ with a resolution of 4 cm$^{-1}$, corrected for dark-current noise, and normalized. The obtained spectra were fitted to get quantitative values for the band areas of heavily overlapped bands. The curve-fitting procedure is based on a least-squares minimization which in its turn involves entering the values of the wavenumbers of the component bands (determined by using deconvolution) and then a program determines the best estimated parameters of the component curves. The deconvolution process involves several steps: computation of an interferogram of the sample by computing the inverse Fourier-transform of the spectrum, multiplication of the interferogram by a smoothing function and a function consisting of a Gaussian–Lorentzian band shape, and Fourier transformation of the modified interferogram. The deconvolution procedure is typically repeated iteratively to obtain the best results. At iteration, the line shape is adjusted to provide narrower bands without excessive distortion. Therefore, each Raman spectra has its characteristic peak positions.

## 3. Results and discussion

### 3.1. Structure analysis of CuSe thin films

X-ray diffraction (XRD) pattern of CuSe thin film of thickness 172.7 nm (as a representative example) was shown in Fig. 1. The smoothed spectrum declares the absence of any sharp diffraction lines, indicating the amorphous nature of the as-deposited film. The EDX diagrams of CuSe thin film of thickness 172.7 nm (not shown) possess a nearly stoichiometric composition (Cu = 50 ± 2%, Se = 50 ± 2%).

### 3.2. Optical properties of CuSe thin films

The spectral distribution of $T(\lambda)$ and $R(\lambda)$ were studied for CuSe films of thicknesses (56.75, 79.74 and 172.70 nm) in the wavelength range (380–1700 nm) are illustrated in Fig. 2. The refractive index $n$ and absorption index $k$ were calculated automatically using F10-VC-EXR software for the investigated thicknesses. The spectral distribution of $n$ and $k$ as a function of wavelength $\lambda$ for the investigated compound indicated that their variation with film thickness lies within the experimental error. Accordingly, both $n$ and $k$ are

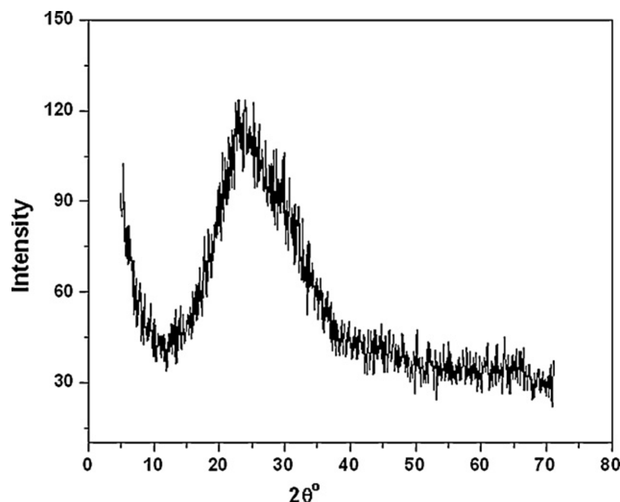


**Fig. 1.** X-ray diffraction pattern of the as-deposited CuSe thin film of thickness 172.7 nm (as a representative example).

independent of the film thickness. For that reason, the values of the spectral distribution of $n(\lambda)$ and $k(\lambda)$ versus wavelength of thickness 172.70 nm was taken as a representative example as shown in Fig. 3. Both the refractive index and the absorption index decrease with increasing the wavelength for the investigated thin film. But, the refractive index $n$ attain a peak at a wavelength $\lambda$ = 505 nm laying in the absorption region, but at higher wavelength, $n(\lambda)$ tends to be constant i.e. the film become non-dispersive. We can conclude that, the refractive index shows an anomalous dispersion at the lower wavelengths and a normal dispersion at the higher wavelengths.

The refractive index dispersion has been analysed using the concept of Wemple and Didomenico (WDD) single oscillator model [13,14]. In this concept, the dispersion energy parameters $E_d$ and $E_o$ are introduced and the optical data could be described to an excellent approximation by the following expression:

$$(n^2 - 1)^{-1} = \frac{E_o}{E_d} + \frac{1}{E_o E_d}(h\nu)^2, \quad (1)$$

where $h$ is Planck's constant, $\nu$ is the frequency, $h\nu$ is the photon energy. The physical meaning of $E_d$ is related to the average strength

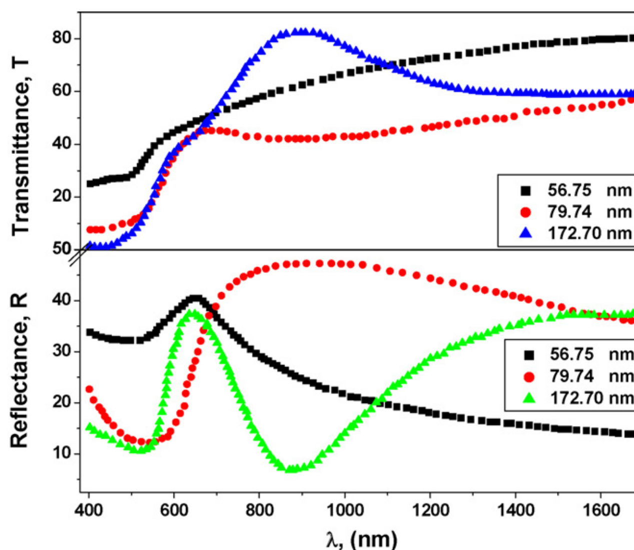


**Fig. 2.** The spectral distribution curves of the experimental $T(\lambda)$ and $R(\lambda)$ of CuSe films.

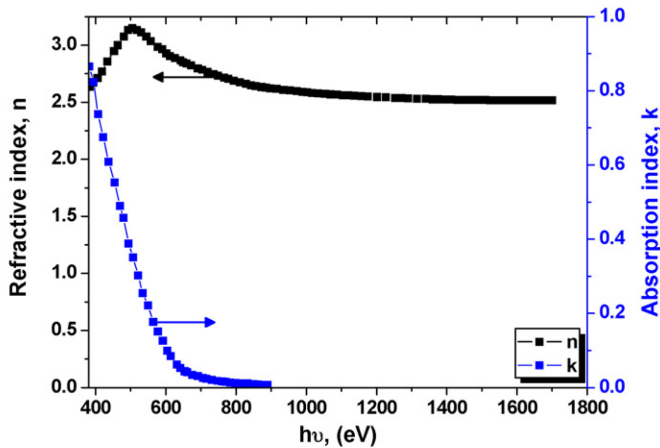


**Fig. 3.** Dependence of the refractive index $n$ and the absorption index $k$ on the wavelength $\lambda$ for CuSe film of thickness 172.7 nm.

of interband optical transitions and is associated with the changes in the structural order of the material and the effective oscillator energy, while $E_o$ can directly correlate with the optical energy gap by an empirical formula. $E_o$ is considered as an average bandgap, the so-called WDD bandgap, and it corresponds to the distance between the 'centers of gravity' of the valence and the conduction bands: $E_o$ is, therefore, related to the bond energy of the different chemical bonds present in the material. Experimental verification of Eq. (1) can be obtained by plotting $(n^2-1)^{-1}$ versus $(h\nu)^2$ for CuSe thin film (not shown). It is observed that the plot is linear over all the range from 0.5 to approximately 1.5 eV. The determination of $E_o$ and $E_d$ were estimated by a linear fitting using a plotting program. Values of $E_o$ and $E_d$ equal 3.91 and 19.99 eV, respectively. The oscillator energy $E_o$ is an average energy gap and in a close approximation with the optical bandgap $E_g^{\text{opt}}$, in which, $E_o \approx 1.5E_g^{\text{WDD}}$, as suggested by WDD model [13,14]. The value of the optical bandgap from WDD model equals 2.61 eV. The refractive index $n_o$ (at zero photon energy) is calculated by extrapolating the WDD dispersion equation to $h\nu \to 0$ (the static refractive index), which is defined by the infinite wavelength dielectric constant $\varepsilon_\infty^{\text{WDD}} = n_0^2$, can be deduced from the dispersion relationship as follows:

$$n_o^2 = \left(1 + \frac{E_d}{E_o}\right), \tag{2}$$

The value of $n_o$ equals 2.47 and hence, the value of $\varepsilon_\infty^{\text{WDD}} \approx 6.1$.

The obtained data of refractive index $n$ can be analyzed to obtain the high frequency dielectric constant $\varepsilon_\infty$ via two different methods [7–10]. To obtain a reliable value of the high frequency dielectric constant $\varepsilon_\infty$, we employed both procedures. The first method describes the contribution of the free carriers and the lattice vibration modes of the dispersion. The following equation can be used to obtain the high frequency dielectric constant [15–18]:

$$\varepsilon_1 = \varepsilon_{\infty(1)} - B\lambda^2, \tag{3a}$$

and:

$$B = \frac{e^2 N}{4\pi^2 c^2 \varepsilon_o m^*}, \tag{3b}$$

where $\varepsilon_1$ is the real part of dielectric constant, $\varepsilon_{\infty(1)}$ is the lattice dielectric constant (the high frequency dielectric constant according to first procedure), $\lambda$ is the wavelength, $N$ is the free charge carrier concentration, $\varepsilon_o$ is the permittivity of free space, $m^*$ is the effective mass of the charge carrier and $c$ is the velocity of light. The real part of dielectric constant $\varepsilon_1 = n^2$ was calculated at different values of $\lambda$ in the transparent region ($k = 0$). Then, the obtained values of $\varepsilon_1$ are plotted as a function of $\lambda^2$ (not shown). It is observed that the dependence of $\varepsilon_1$ on $\lambda^2$ is linear at the longer wavelengths (transparent region). Extrapolating of the linear part of this dependence to zero wavelength gives the value of $\varepsilon_{\infty(1)}$ and from the slope of this line, value of $N/m^*$ for the investigated CuSe thin film was calculated according to the Eq. (3b). The obtained values of $\varepsilon_{\infty(1)}$ and $N/m^*$ are given in Table 1. It is known that in the range of transparency, when the electron damping parameter $\gamma < \omega$ [19], the dielectric constant can be written as:

$$\varepsilon_1 = \varepsilon_{\infty(1)} - \frac{\omega_p^2}{\omega^2}, \tag{4a}$$

and:

$$\omega_p^2 = \frac{e^2 N/m^*}{\varepsilon_o}, \tag{4b}$$

where $\omega_P$ is the plasma frequency and $\omega$ is the incident light frequency. The calculated value of the $\omega_P$ is given in Table 1.

The second procedure is based upon the dispersion arising from the bound carriers in an empty lattice. The model of Moss [20], which stated that the free carrier contributions to dispersion are relatively small. The properties of the investigated sample could be treated as a single oscillator of wavelength $\lambda_o$ at the higher frequency. The high frequency dielectric constant can be calculated by applying the following simple classical dispersion relation [15–18]:

$$\frac{(n_\circ^2-1)}{(n^2-1)} = 1 - \left(\frac{\lambda_o}{\lambda}\right)^2, \tag{5}$$

where $n_o$ is the refractive index at infinite wavelength $\lambda_o$ (average interband oscillator wavelength), $n$ is the refractive index and $\lambda$ is the wavelength of the incident photon. Plotting of $(n^2-1)^{-1}$ against $\lambda^{-2}$ (not shown) showed a linear part (below the absorption edge). The intersection with $(n^2-1)^{-1}$ axis is $(n_0^2-1)^{-1}$ and the slope of the extrapolated line equals $\lambda_0^2/(n_0^2-1)^{-1}$ and hence, $\varepsilon_{\infty(2)} = n_0^2$ at $\lambda_o$ (the high frequency dielectric constant according to the second procedure). The obtained value of $\varepsilon_{\infty(2)}$ is given in Table 1. Eq. (5) can also be rewritten as [14,21]:

$$(n^2-1) = \left(\frac{S_o {\lambda_o}^2}{1-(\lambda^2/\lambda_o^2)}\right), \tag{6a}$$

where $S_o$ is the average oscillator strength which equals to:

$$S_o = \frac{(n_0^2-1)}{\lambda_o^2}, \tag{6b}$$

Value of $S_o$ and $E_o/S_o$ at the given values of $n_0^2$ and $\lambda_o$ are calculated and given in Table 1. This value is approximately in the same order as that obtained by WDD [13,14] for a number of materials.

It is clear that the values of $\varepsilon_{\infty(1)}$ and $\varepsilon_{\infty(2)}$ obtained from the two procedures are approximately equal, this may be attributed to the lattice vibrations and bounded carriers in an empty lattice are in the transparent region [17,22]. The mean values of the high frequency dielectric constant $\varepsilon_\infty$ for CuSe equal $4.26 \pm 0.14$. Values of $\varepsilon_\infty^{\text{WDD}}$ are in good agreement with those values of $\varepsilon_{\infty(1)}$ and $\varepsilon_{\infty(2)}$.

**Table 1**
Values of $\varepsilon_{\infty(1)}$, $\varepsilon_{\infty(2)}$, $\lambda_o$, $S_o$, $E_o/S_o$, $\omega_p$, and $N/m^*$ for CuSe thin films.

| Material | From Fig. 5 $\varepsilon_{\infty(1)}$ | From Fig. 6 $\varepsilon_{\infty(2)}$ | $\lambda_o$, nm | $S_o$, $m^{-2}$ | $E_o/S_o$, eV $m^2$ | $\omega_P$, Hz | $N/m^*$, $m^{-3}$ $gm^{-1}$ |
|---|---|---|---|---|---|---|---|
| CuSe | 6.4 | 6.12 | 845.28 | $5.1 \times 10^{13}$ | $7.67 \times 10^{-14}$ | $2.46 \times 10^{14}$ | $2.09 \times 10^{56}$ |

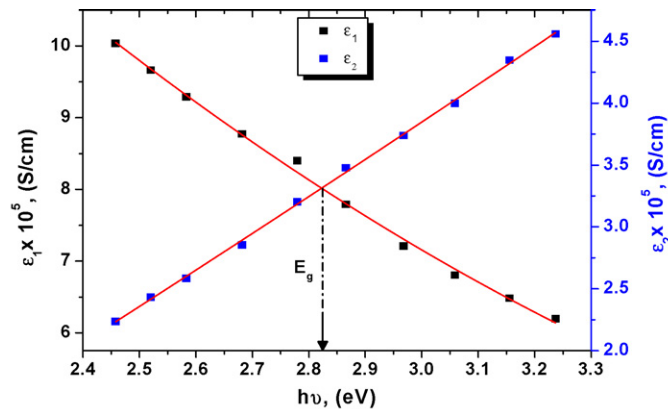


**Fig. 4.** Dependence of the real and imaginary parts of the dielectric constant on the photon energy $h\nu$ for CuSe thin films.

The complex refractive index $\hat{n} = n(\lambda) + ik(\lambda)$ and the dielectric function $\hat{\varepsilon} = \varepsilon_1(\lambda) + i\varepsilon_2(\lambda)$ characterize the optical properties of any solid material. The imaginary and real parts of dielectric constant were determined by the following relations in the absorption region ($k \neq 0$) [2,8,17,23,24]:

$$\varepsilon_1 = n^2 - k^2 = \varepsilon_\infty - \left(\frac{e^2 N}{4\pi^2 c^2 \varepsilon_o m^*}\right)\lambda^2, \quad (7)$$

and:

$$\varepsilon_2 = 2nk = \left(\frac{\varepsilon_\infty \omega_p^2}{8\pi^2 c^3 \tau}\right)\lambda^3, \quad (8)$$

where $\varepsilon_1$ is the real part (represents the normal dielectric constant), $\varepsilon_2$ is the imaginary part of the dielectric constant (represents the absorption associated of radiation by free carrier), $\tau$ is the optical relaxation time and $k = \alpha\lambda/4\pi$ is the absorption index. The real and imaginary parts of the dielectric constant of the investigated films are shown in Fig. 4. Value of the optical bandgap $E_g$ can be evaluated from this plot by extrapolation a straight line from the cross-point between the obtained curves of the real and imaginary parts of the dielectric constant to the $x$-axis which equal approximately 2.82 eV.

The dielectric relaxation time $\tau$ can be determined by the following equation [25–27]:

$$\tau = \left|\frac{\varepsilon_\infty - \varepsilon_1}{\omega\varepsilon_2}\right|, \quad (9)$$

The modulus was taken for Eq. (9) because the value of $\varepsilon_\infty$ is always less than the values of $\varepsilon_1$. Fig. 5 depicts the dielectric relaxation time $\tau$ as a function of photon energy $h\nu$ for CuSe films. Value of the optical bandgap $E_g$ can be evaluated throughout this plot from the cross-point between the tangent of the plot of lower and higher values of the photon energy of the calculated relaxation time to the $x$-axis, and the obtained value of $E_g \approx 2.74$ eV.

In physics, the dissipation factor $\tan\delta$ is a measure of loss-rate of power of a mechanical mode, such as an oscillation, in a dissipative system. For example, electric power is lost in all dielectric materials, usually in the form of heat. The dissipation factor $\tan\delta$ can be calculated according to the following equation [2,22]:

$$\tan\delta = \frac{\varepsilon_2}{\varepsilon_1}, \quad (10)$$

The variation of $\tan\delta$ for the investigated films with $h\nu$ is shown in Fig. 6. It is found that the dissipation factor increases with increasing the photon energy.

The complex optical conductivity ($\sigma^* = \sigma_1(\lambda) + i\sigma_2(\lambda)$) is related to the complex dielectric constant ($\varepsilon^* = \varepsilon_1(\lambda) + i\varepsilon_2(\lambda)$) by the relation [28]:

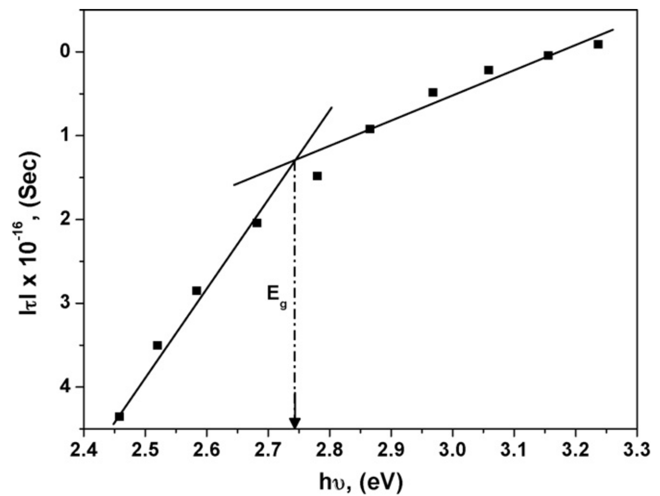


**Fig. 5.** Dependence of the dielectric relaxation time $\tau$ on the photon energy $h\nu$ for CuSe thin films.

$$\sigma_1 = \omega\varepsilon_2\varepsilon_0, \quad (11)$$

$$\sigma_2 = \omega\varepsilon_1\varepsilon_0, \quad (11a)$$

The real $\sigma_1$ and imaginary $\sigma_2$ parts of the optical conductivity as a function of the photon energy are shown in Fig. 7. It is clear from this figure that the real part decreases with increasing the photon energy while the imaginary part increases with increasing the photon energy. Value of the optical bandgap $E_g$ can be evaluated from the cross-point between the curves of the real and imaginary parts of the optical conductivity to the $x$-axis, value of $E_g \approx 2.86$ eV.

The absorption coefficient $\alpha$ is calculated from the well-known equation, $\alpha = 4\pi k/\lambda$. The spectral behavior of the absorption coefficient $\log\alpha$ as a function of $h\nu$ for CuSe thin films is illustrated in Fig. 8. The interband transition in amorphous solid is characterized by a slow rise in the absorption coefficient with photon energy. The optical bandgap and the nature of optical transitions can be obtained from the dependence of the absorption coefficient on the photon energy. The absorption coefficient of chalcogenide semiconductors is known to change rapidly for photon energies close

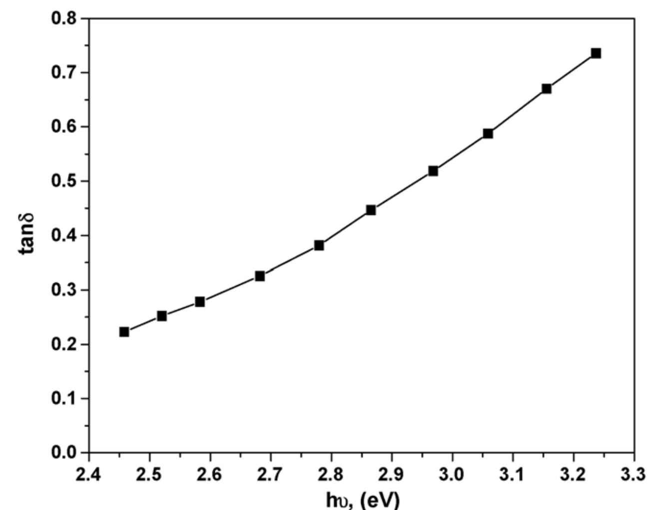


**Fig. 6.** Dependence of the dissipation factor $\tan\delta$ on the photon energy $h\nu$ for CuSe thin films.

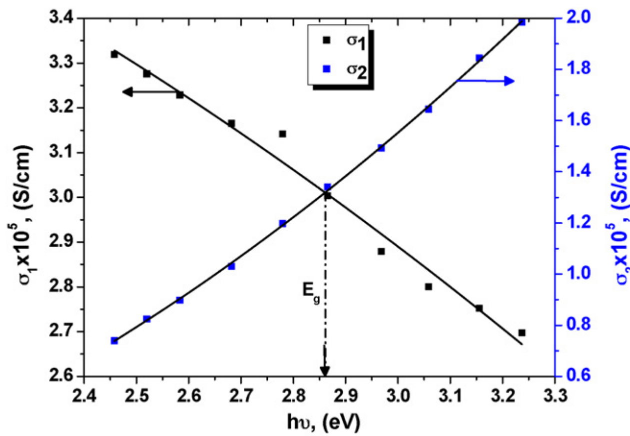


**Fig. 7.** Dependence of the real and imaginary parts of the optical conductivity on the photon energy $h\nu$ for CuSe thin films.

to their bandgap and can be divided into two regions according to the values of absorption coefficient [29,30]. The first region for the higher values of the absorption coefficient, $\alpha > 10^4$ cm$^{-1}$, the optical absorption edge was analyzed by the Tauc power law for the direct optical transition according to the value of $m$ as follows [22,31–34]:

$$\alpha h\nu = A(h\nu - E_g)^m \quad (12)$$

where $A$ is constant (the edge width parameter representing the film quality), $E_g$ is the optical energy gap and $m$ determines the type of the optical transition. Plotting of $(\alpha h\nu)^2$ versus $h\nu$ is shown in Fig. 9. Value of the energy gap $E_g$ is determined by extrapolation of the two linear parts of this curve to the $x$-axis for the as-deposited CuSe thin films. Accordingly, values of $E^{d.}_{g(1)}$ and $E^{d.}_{g(2)}$ of CuSe thin film equal 2.7 eV and 2.33 eV, respectively which is in good agreement with the values obtained by Biljana Pejova and Ivan Grozdanov [30], Mondal and Pramanik [35].

For the second region, ($\alpha < 10^4$ cm$^{-1}$), the absorption at the lower photon energy usually follows the Urbach's rule [22,31,32] according to the following equation:

$$\alpha(\nu) = \alpha_o \exp\left(\frac{h\nu}{E_e}\right), \quad (13)$$

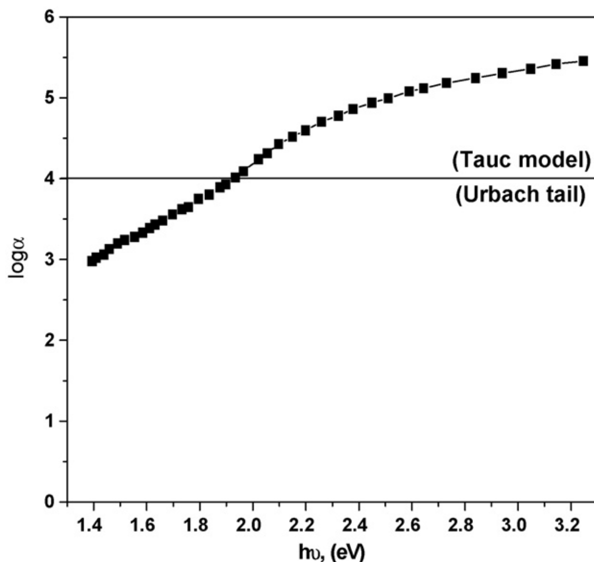


**Fig. 8.** Dependence of the absorption coefficient $\log\alpha$ on the photon energy $h\nu$ for CuSe thin films.

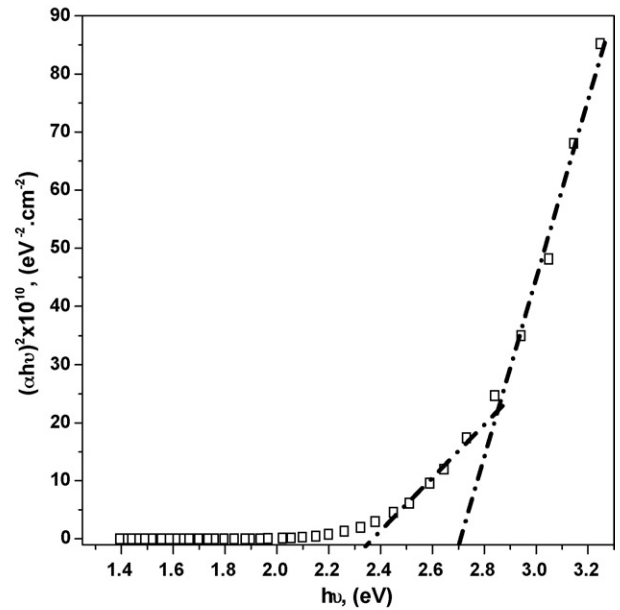


**Fig. 9.** Dependence of $(\alpha h\nu)^2$ on the photon energy $h\nu$ for the as-deposited thin films.

where $\nu$ is the frequency of the radiation, $\alpha_o$ is a constant, $h$ is the Planck's constant and $E_e$ is Urbach's energy which is interpreted as the width of the tails of localized states in the bandgap and in general represents the degree of disorder in the amorphous semiconductors [29]. The absorption in this region is due to the transitions between extended states in one band and localized states in the exponential tail of the other band. From plotting of $\log\alpha$ as a function of $h\nu$ as shown in Fig. 8, values of $E_o$and $\alpha_o$ can be calculated and equal 0.54 eV and 2.63 cm$^{-1}$, respectively for the investigated films.

### 3.3. Raman spectral studies

The Raman spectroscopy of the CuSe thin film was analyzed in the spectrum range 100–800 cm$^{-1}$. Peaks were initially set to the positions mentioned above and the fit was done using with Gaussian–Lorentzian bands until the band sum deviation from

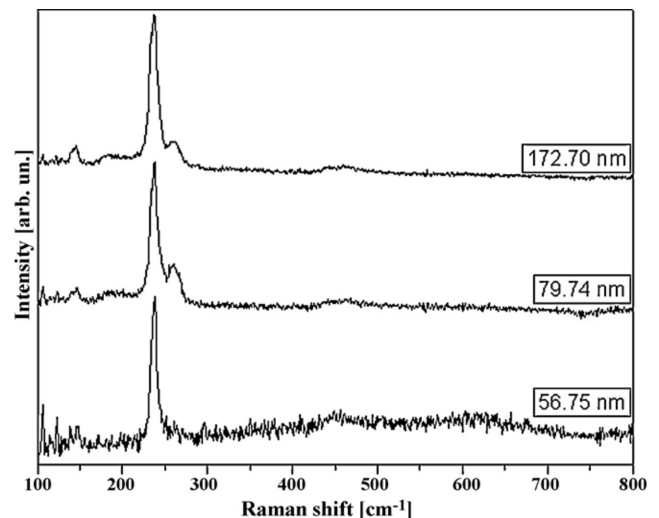


**Fig. 10.** Raman spectra of CuSe thin films of different thicknesses.

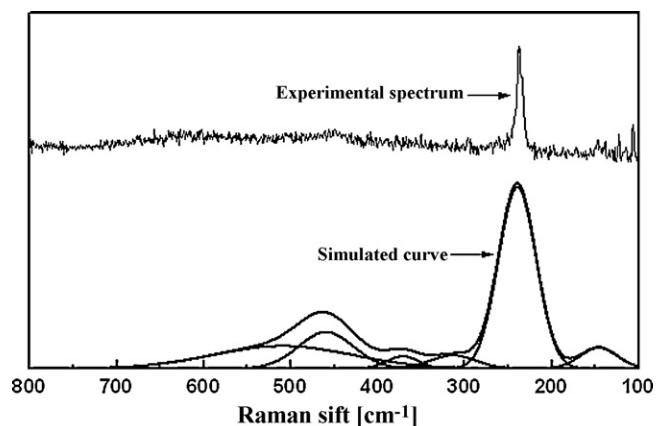


**Fig. 11.** The curve fitting spectrum of Raman spectrum of CuSe film of thickness 56.75 nm (as a representative example), and the difference between the experimental and simulated curves.

**Table 2**
The band fitting of the Raman spectra.

| Thickness | | | | | | | |
|---|---|---|---|---|---|---|---|
| 56.75 nm | | | | | | | |
| *I* | 0.1 | | 1 | 0.1 | 0.1 | 0.2 | 0.1 |
| *C* | 145 | | 239 | 313 | 371 | 459 | 509 |
| *A* | 5.6 | | 50 | 4.4 | 2.8 | 14.7 | 22.7 |
| 79.74 nm | | | | | | | |
| *I* | | 0.4 | 0.7 | | 0.1 | 0.1 | |
| *C* | | 228 | 250 | | 347 | 455 | |
| *A* | | 33 | 49 | | 7.8 | 10.3 | |
| 172.70 nm | | | | | | | |
| *I* | 0.1 | 0.3 | 0.9 | 0.2 | 0.1 | 0.1 | |
| *C* | 148 | 218 | 240 | 262 | 344 | 456 | |
| *A* | 8.4 | 12.3 | 53 | 9.2 | 8 | 9.2 | |

*I* is the intensity of the band, *C* is its center, and *A* is its relative area.

experimental spectrum was less than 1%. Intensities of peaks were measured over the baseline and were normalized to the most intense peak [36]. The Raman spectra of CuSe films of different thicknesses are shown in Fig. 10. One can observe that the presence of three main intense and broad peaks. The first is situated at 145.527 $cm^{-1}$, the second at 237.751 $cm^{-1}$ and the third at 260.468 $cm^{-1}$. The first and third peaks are weak comparing with the main peak observed at 237.751 $cm^{-1}$.

The elementary selenium is identified by the peak at 240 $cm^{-1}$ which is due to trigonal selenium [36,37], one can observe a peak at 237.751 $cm^{-1}$ in Fig. 10 confirming the above mentioned. Copper selenide is identified at 260.648 $cm^{-1}$ from the spectrum in which the reported peak at 259 $cm^{-1}$ is the most intense peak observed on Raman spectrum of CuSe [36,37] which corresponds to Cu–Se vibration and is in good agreement with the literature [38,39].

The observed broadening of the bands in the Raman spectra of the studied compound may be arising from the overlapping of some individual bands with each other. Each individual band has two characteristic parameters; the center (*C*), which is related to some type of vibrations of a specific structural group and the relative area (*A*), which is proportional to the concentration of this structural group. A curve fitting process should be performed to extract such parameters [40,41]. Fig. 11 shows the fitting spectrum of the thickness 56.75 nm (as a representative example), and the difference between the experimental and simulated curves. The characteristic parameters of each band of the Raman spectra are given in Table 2.

## 4. Conclusions

The structural, optical dispersion parameters and the Raman spectroscopy have been studied for CuSe thin films. X-ray diffraction results indicate that CuSe thin films have an amorphous structure. The refractive index shows an anomalous dispersion at the lower wavelength (absorption region) and a normal dispersion at the higher wavelengths (transparent region). The refractive index dispersion obeys the single oscillator model proposed by Wemple and DiDomenico WDD and the single oscillator parameters were determined. The bandgap of CuSe thin films was determined by three novel methods i.e. ((real and imaginary) dielectric constant, relaxation time and (real and imaginary) optical conductivity) which in a good agreement with the Tauc bandgap (2.7 eV).

## References


[1] A. Ahmad, S.A. Khan, A.A. Al-Ghamdi, F.A. Al-Agel, K. Sinha, M. Zulfequard, M. Husain, J. Alloys Compd. 497 (2010) 215–220.
[2] M. Fadel, S.A. Fayek, M.O. Abou-Helal, M.M. Ibrahim, A.M. Shakra, J. Alloys Compd. 485 (2009) 604–609.
[3] G.H. Yue, W. Wang, L.S. Wang, X. Wang, P.X. Yan, Y. Chen, D.L. Peng, J. Alloys Compd. 474 (2009) 445–449.
[4] D. Zhao, X. Zhang, H. Wang, H. Zeng, H. Ma, J.L. Adam, G. Chen, J. Non-Cryst Solids 354 (2008) 1281.
[5] G. Dong, H. Tao, X. Xiao, S. Gu, Mater. Res. Bull. 42 (2007) 1804.
[6] K.T. Liu, J.G. Duh, J. Non-Cryst. Solids 353 (2007) 1060.
[7] A.A. Abu-Shely, A.A. Elabbar, Physica B 390 (2007) 196.
[8] S.A. Khan, F.S. Al-Hazmi, S. Al-Heniti, A.S. Faidah, A.A. Al-Ghamdi, Curr. Appl. Phys. 10 (2010) 145–152.
[9] E. Abd El-Wahabb, A.M. Farid, J. Alloys Compd. 472 (2009) 352–357.
[10] P.P. Hankare, A.S. Khomane, P.A. Chate, K.C. Rathod, K.M. Garadkar, J. Alloys Compd. 469 (2009) 478–482.
[11] S.R. Gosavi, N.G. Deshpande, Y.G. Gudage, R. Sharma, J. Alloys Compd. 448 (2008) 344–348.
[12] K. Liu, H. Liu, J. Wang, L. Shi, J. Alloys Compd. 484 (2009) 674–676.
[13] S.H. Wemple, M. DiDomenico, Phys. Rev. B 3 (1971) 1338.
[14] S.H. Wemple, Phys. Rev. B 7 (1973) 3767.
[15] J.N. Zemel, J.D. Jensen, R.B. Schoolar, Phys. Rev. A 140 (1965) 330.
[16] E.G. El-Metwally, M.O. Abou-Helal, I.S. Yahia, J. Ovonic Res. 4, 2 (2008) 20–34.
[17] M.M. Abdel-Aziz, I.S. Yahia, L.A. Wahab, M. Fadel, M.A. Afifi, Appl. Surf. Sci. 252 (2006) 8163–8170.
[18] O.A. Azima, M.M. Abdel-Azizb, I.S. Yahia, Appl. Surf. Sci. 255 (2009) 4829–4835.
[19] M.M. El-Nahass, M.M. Sallam, S.A. Rahman, E.M. Ibrahim, Solid State Sci. 8 (2006) 488–499.
[20] T.S. Moss, Optical Properties of Semiconductors, Butter Worths Scientific Publication Ltd., London, 1959.
[21] F. Yakuphanoglu, A. Cukurovali, I. Yilmaz, Physica B 351 (2004) 53.
[22] M.M. Abdel-Aziz, E.G. El-Metwally, M. Fadel, H.H. Labib, M.A. Afifi, Thin Solid Films 386 (2001) 99.
[23] A. El-Korashy, H. El-Zahed, M. Radwan, Physica B 334 (2003) 75.
[24] M.M. Wakad, E.Kh. Shokr, S.H. Mohammed, J. Non-Cryst. Solids 265 (2000) 157.
[25] R.J. Bell, M.A. Ordal, R.W. Alexender, Appl. Opt. 24 (1985) 3680.
[26] M.Y. Han, H. Huang, C.H. Chew, L.M. Gan, X.J. Zhang, W. Ji, J. Phys. Chem. B 102 (1998) 1884.
[27] M.M. El-Nahass, A.A.M. Faraga, E.M. Ibrahim, S. Abd-El-Rahman, Vacuum 72 (2004) 453–460.
[28] F. Yakuphanoglu, M. Sekerci, O.F. Ozturk, Opt. Commun. 239 (2004) 275–280.
[29] Pankaj Sharma, S.C. Katyal, Mater. Chem. Phys. 112 (2008) 892–897.
[30] B. Pejova, I. Grozdanov, J. Solid State Chem. 158 (2001) 49–54.
[31] N. Kenny, C.R. Kannewurf, D.H. Whitmore, J. Phys. Chem. Solids 27 (1966) 1237.
[32] N.F. Mott, E.A. Davis, Electronic Process in Non-Crystalline Materials, Calendron Press, Oxford, 1979.
[33] S.A. Khan, J.K. Lal, A.A. Al-Ghamd, Opt. Laser Technol. 42 (2010) 839–844.
[34] M.A. Majeed Khan, M. Wasi Khan, M. Husain, M. Zulfequar, J. Alloys Compd. 486 (2009) 876–880.
[35] A. Mondal, P. Pramanik, J. Solid State Chem. 47 (1983) 81–83.
[36] O. Ramdani, J.F. Guillemoles, D. Lincot, P.P. Grand, E. Chassaing, O. Kerrec, E. Rzepka, Thin Solid Films 515 (2007) 5909–5912.
[37] P. Nagels, E. Sleeckx, R. Callaerts, L. Tichy, Solid State Commun. 94 (1995) 49.
[38] E. Motohiko shii, K. Shibata, H. Nozaki, J. Solid State Chem. 105 (1993) 504.
[39] B. Minceva-Sukarova, M. Najdoski, I. Grozdanov, C.J. Chunnilall, J. Mol. Struct. 410–411 (1997) 267–270.
[40] Y. Saddeek, M.S. Gaafar, A. Safaa, Bashier, J. Non-Cryst. Solids 356 (2010) 1089.
[41] I.S. Yahia, Y.B. Saddeek, G.B. Sakr, W. Knoff, T. Story, N. Romčević, W. Dobrowolski, J. Magn. Magn. Mater. 321 (2009) 4039.